Check for
updates

Investigation on physico-mechanical properties and microstructural evolution patterns of heated granite after liquid nitrogen cooling

Zhouqian Wu · Minghui Li · Heping Xie · Jun Lu · Cancan Chen

Abstract Liquid nitrogen (LN_2) fracturing is recognized as an innovative reservoir enhancement technique, demonstrating significant potential in establishing high permeability pathways in geothermal development. Understanding the physico-mechanical properties and microscopic mechanisms of hot dry rock post LN_2 cooling treatment is pivotal for promoting the effective deployment of LN_2 fracturing. This study undertook physical and mechanical testing on a quintessential hot dry rock type-granite-post various temperature and LN_2 cooling treatments. Subsequently, a multi-scale investigation was conducted on the thermal fracture-pore structure's morphological features and the evolution of mineral components. The experimental findings indicated that LN_2 cooling exerts a pronounced impact on the physico-mechanical properties of high-temperature granite.

Temperature-induced damage to granite can be delineated into three phases: initial phase up to 200 °C where its effects are relatively imperceptible; an intermediate phase from 200 to 500 °C characterized by gradual deterioration; and a pronounced degradation phase evident at 600 °C. Correlations between the changes in the micro pore-fracture structure of granite and its physico-mechanical property degradation were subsequently established. As temperature escalated, the area of micro-defects in the CT-reconstructed spatial distribution increased progressively. The volumetric porosity damage ratio and fractal dimensions were quantitatively introduced to characterize the fractal geometric features and distribution patterns of internal thermal fractures in granite post thermal shock. Concurrently, NMR experiments indicated that with the escalation of temperature, micropore develop and interlink to form mesopore and macropore, enhancing rock porosity connectivity. These macropores significantly influence granite's physico-mechanical and permeability characteristics. A mineral stability analysis revealed that various minerals undergo physico-chemical reactions, such as dehydration, phase transitions, decomposition, and chemical bond fractures at elevated temperatures, altering mineralogical composition and mineral strength, thus impacting the rock's macroscopic properties. Ultimately, the study delved into the damage mechanisms of granite's physico-mechanical properties from both heating and cooling perspectives during various temperature phases. The insights garnered from this investigation offer novel

Z. Wu · *Present Address:*
M. Li (✉) · H. Xie · J. Lu · C. Chen
State Key Laboratory of Intelligent Construction and Healthy Operation and Maintenance of Deep Underground EngineeringCollege of Civil and Transportation Engineering, Shenzhen University, Yuehai Campus: 3688 Nanhai Avenue, Nanshan District, Shenzhen 518060, China
e-mail: mhli@szu.edu.cn

Z. Wu · M. Li · H. Xie · J. Lu · C. Chen
Guangdong Provincial Key Laboratory of Deep Earth Sciences and Geothermal Energy Exploitation and Utilization, Institute of Deep Earth Sciences and Green Energy, Shenzhen University, Shenzhen 518060, China

✌ Springer

value in comprehending the thermal damage characteristics induced by LN_2 cooling.

Article Highlights

1. Investigated the physico-mechanical properties of granite post liquid nitrogen cooling under varying temperature treatments.
2. Elucidated the development and evolutionary patterns of pore-fracture structures through microscopic experimentation.
3. Established the connection between microscopic and macroscopic properties.

Keywords Hot dry rock · Physical and mechanical properties · LN_2 cooling · Microscopic observation

1 Introduction

Geothermal energy stored in hot dry rock (HDR) represents a burgeoning renewable resource, boasting numerous advantages such as reduced carbon emissions, vast application prospects, and widespread distribution in comparison to conventional fuels like natural gas, petroleum, and coal (Pan et al. 2019, Anderson and Rezaie 2019, Xie et al. 2023). HDR is an intrinsically compacted geological formation situated at depths ranging from 3 to 10 km, exhibiting temperatures between 150 and 600 °C, and is predominantly devoid of water or steam content. This rock formation is primarily composed of granite (Breede et al. 2013). However, the intrinsic structure of HDR reservoir rocks is notably compact, exhibiting minimal permeability, which impedes the fluid flow and heat transfer within the reservoir (Asai et al. 2019). Hence, prior to geothermal extraction, it becomes imperative to enhance the reservoir's permeability either through physical or chemical stimulation. The prevalent method, hydraulic fracturing, is employed to enhance the permeability of the reservoir rocks (Kumari et al. 2018), a technique ubiquitously adopted across the oil, shale gas, and geothermal industries. However, hydraulic fracturing possesses certain undeniable disadvantages, such as significant water resource depletion, environmental contamination, and the inescapable issue of clay hydration expansion (Wang et al. 2016; Li et al. 2016). Additionally, traditional hydraulic fracturing often fails to generate intricate fracture networks. Addressing these challenges, liquid nitrogen (LN_2) fracturing, as an advanced waterless fracturing technique, has been demonstrated to possess immense potential in establishing high-permeability pathway (Li et al. 2016; Wu et al. 2021). LN_2 fracturing was first proposed by McDaniel et al. (1997) in 1990s for treating coal-bed methane reservoirs, is now extensively applied in fracturing unconventional reservoirs. Owing to the extremely low temperature of LN_2 (− 196 °C), when engaged in thermal exchange with the high-temperature reservoir, the resultant temperature differential induces intense thermal stress within the rock. Consequently, during the fracturing procedure, the reservoir undergoes significant thermal damage. This not only enhancement has improved the connectivity of the internal structure, significantly increasing the permeability of the reservoir rock, but also results in internal fracturing of the rock, precipitating a degradation of its physico-mechanical properties, thereby reducing its fracture pressure. Therefore, investigating the physico-mechanical attributes and flow characteristics of granite post-LN_2 cooling, alongside elucidating the microscopic mechanisms of thermal damage, holds paramount importance for guiding engineering practices.

Previous investigations extensively examines the physico-mechanical characteristics of high-temperature granite under both natural and water cooling processes. The density (Zhu et al. 2018), P-wave velocity (Hu et al. 2021), tensile strength (Jin et al. 2019), and uniaxial compressive strength (Jin et al. 2019; Hu et al. 2021) of cooled granite diminish as temperature rises, while porosity (Tang et al. 2019) and permeability (Jin et al. 2019) incrementally increase. The influence of temperature on granite is not a straightforward linear relationship. At specific temperature thresholds, there is a noticeable alteration in the rate of change of the granite's physico-mechanical properties. This can be attributed to certain physical or chemical reactions occurring within the rock at these temperatures, or a significant transformation in its internal structure. For instance, at a particular temperature, certain minerals within the rock may commence melting, crystallizing, or undergoing phase transitions, potentially resulting in rapid alterations

in the rock's strength, elasticity modulus, and other properties. Similarly, upon reaching another temperature threshold, other minerals or structures may initiate reactions, leading to another shift in the property change rate. At the microscale, the observation primarily involves using XRD and SEM to assess the impact of thermal damage on mineral content and mineral structure. There is limited research dedicated to quantitatively analyzing the connection between the microscale and macroscale (Sun et al. 2017; He et al. 2023). Research on the physico-mechanical properties after LN_2 cooling is relatively limited. Cai et al. (2014) investigated the effects of LN_2 cooling on the pore structure of naturally occurring rocks. Their study revealed that LN_2 cooling escalated the internal fracturing of the rock, enhancing crack quantity and opening. Wu et al. (2019a, b) assessed the physico-mechanical damage to rocks at different temperatures post LN_2 cooling. Their findings indicated that after LN_2 cooling, the permeability of heated granite notably increased, while its density, P-wave speed, strength, and elastic modulus decreased. A rise in temperature transitioned the granite from a brittle to a ductile state. Sha et al. (2020) discerned 400 °C as the threshold temperature for LN_2-cooled granite. Beyond this temperature, the rock's physico-mechanical attributes experienced more conspicuous alterations. Microscopic analysis confirmed that the inception and growth of micro-cracks were responsible for the macroscopic property degradation of the rock. Wu et al. (2018) conducted experiments with LN_2 jet rock-breaking. They observed that LN_2 could form a mesh-like crack pattern on the rock's impact surface, reducing the threshold pressure for rock fracture during jet impact.

From the aforementioned study, prior research on LN_2-induced cryogenic damage predominantly focuses on the conventional physical properties and uniaxial compression tests of high-temperature granite. In practical engineering contexts, considerations regarding the impact of cooling media on reservoirs should not only focus on the deterioration of fundamental physical properties but also delve into the evolutionary characteristics of the rock's microscale pore-fracture architecture. This comprehensive understanding will offer a scientific foundation for future extraction activities. Conversely, there's a dearth of studies exploring the triaxial compression characteristics of granite under LN_2 cooling, as well as the

evolution of seepage properties under combined temperature and confining pressure conditions. Furthermore, the microscopic mechanisms underlying the damage to high-temperature granite post-LN_2 treatment remain ambiguous. Consequently, a systematic analysis of the impact mechanism of LN_2 cooling on granite is crucial for effective geothermal energy exploitation.

In this study, the impact of thermal shock caused by LN_2 cooling on the structural damage of granite subjected to different temperature treatments was examined through a series of physico-mechanical tests and microscopic observations. While the majority of currently exploited geothermal reservoirs maintain temperatures below 200 °C, advancements in technology and innovative methodologies may, in the future, target deeper and hotter reservoirs. Accordingly, granite samples were heated from room temperature to 600 °C in this study. The physico-mechanical properties of the granite samples, including density, porosity, P-wave velocity, and thermal conductivity, were meticulously measured. To ascertain the strength and deformational behavior of the granite sample, triaxial compression and Brazilian tensile strength test were conducted. Concurrently, the permeability of granite under varying confining pressures was evaluated, elucidating the percolation characteristics post deep-reservoir modification. Distinctly diverging from most existing study, which predominantly focuses on the macroscopic alterations in rock physico-mechanical properties, this study deployed CT scanning, mineralogical composition analysis, and NMR experiments to uncover the microscopic mechanisms dictating the physico-mechanical behavior of granite subjected to LN_2 cooling. Conclusively, the evolution and mechanisms of granite damage were delved into from both heating and cooling perspectives. This research endeavours to pave the way for innovative strategies to augment the production of geothermal energy in HDR reservoirs.

2 Materials and methodology

2.1 Rock specimen preparation

Granite is a typical rock type in HDR systems, and was selected as the experimental material for this study. The rock samples used in the experiment were

**Table 1** Mineralogical composition of granite specimens tested by XRD

Mineral composition	Oligoclase	Microcline	K-feldspar	Quartz	Biotite	Clay
Content (%)	39.7	27.0	26.6	5.4	0.89	0.41

sourced from Hubei Province, China, with an average density of 2.622 g/cm^3. X-ray diffraction (XRD) analysis revealed that the primary mineral constituents of the samples are feldspar and quartz (shown in Table 1). Specimens were prepared in strict accordance with the specifications recommended by the International Society for Rock Mechanics (Ulusay and Hudson 2007), producing cylindrical samples of 50 mm in diameter and 100 mm in height, as well as disc samples of 50 mm in diameter and 25 mm in height. Prior to thermal treatment, the physicomechanical properties of the rock samples were measured and tested. To minimize dispersion in the experimental results, specimens with P-wave velocity and porosity significantly deviating from the mean values were excluded, and the remaining specimens were numbered and grouped accordingly.

2.2 Heating and cooling treatment

To ensure the precision of experimental results, granite specimens were categorized into seven distinct temperature groups, inclusive of ambient conditions. Each group consisted of one cylindrical specimen and one disc specimen. For each temperature group, the samples were subjected to three tests

under identical conditions for their physico-mechanical properties, with the final results calculated as the average of these tests. Initially, the granite samples were heated in a KSL-1300X muffle furnace. Considering that too rapid a heating rate could induce thermal shock in the rock, leading to thermal cracking, this study opted for a slower heating rate. A rate of 5 °C/min was used to heat the granite samples to 150, 200, 300, 400, 500 and 600 °C, respectively. Upon reaching the target temperature, the samples were held at that temperature for 2 h to ensure adequate heating (shown in Fig. 1a). Subsequently, the samples were quickly removed and placed in an insulated container filled with LN$_2$ for 1 h to ensure complete cooling. Notably, in actual engineering practice, when performing LN$_2$ fracturing on geothermal reservoirs, HDR are subjected to two types of thermal shock loads: the freezing process and the thawing process. Since too rapid a temperature recovery rate during the transition from the frozen to thawed state could damage the rock (Hou et al. 2022), the focus of this study is on the impact of rapid cooling on the physico-mechanical properties of granite. Therefore, after thorough cooling, the frozen granite was placed in an insulated container to allow the temperature of the granite
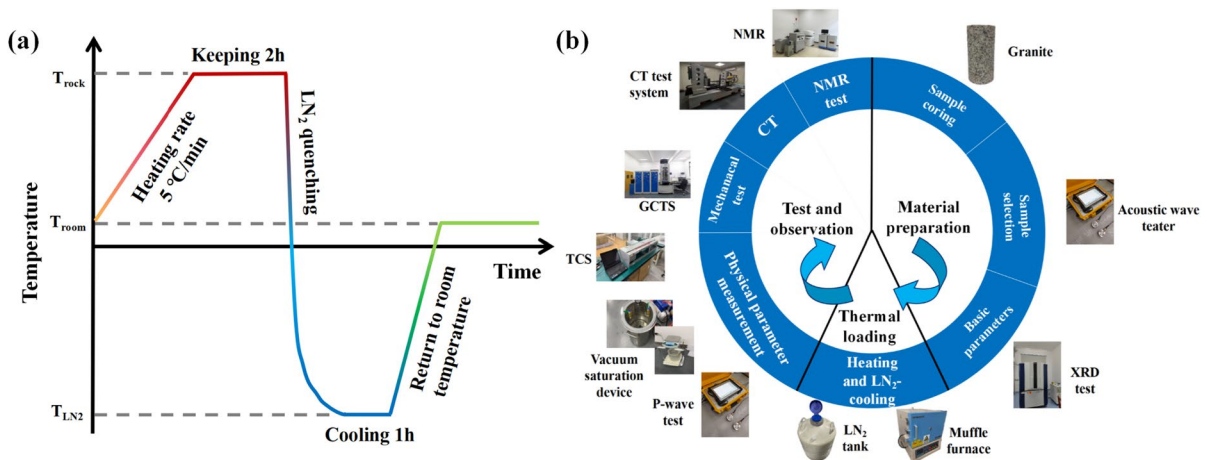
Fig. 1 **a** Thermal heating and LN$_2$ cooling strategy; **b** Experimental procedure and apparatus

to gradually return to room temperature at a slow rate. Following this, the samples treated with LN_2 were dried in a drying oven at 85 °C for 24 h before undergoing tests for their physico-mechanical properties, as depicted in Fig. 1b.

2.3 Physical property tests

Physical property tests were conducted on the heat-treated granite samples, including measurements of density, P-wave velocity, porosity, and thermal conductivity.

Utilizing the principles of the triple-weight method, the density and porosity of specimens, both before and after thermal treatment, can be ascertained (Ulusay and Hudson 2007). Initially, granite specimens are submerged in water under a vacuum pressure of 0.1 MPa for 24 h to ensure saturation. They are subsequently transferred to an alternate water bath, where the mass of the saturated specimen in water, denoted as m_{sat}, is measured using an analytical balance. Following this, specimens are removed from the water, gently dabbed with a paper towel to eliminate excess surface water, and the saturated surface mass, represented as m_{sub}, is recorded. Ultimately, these specimens are dried in an oven at 85 °C for a span of 24 h, after which they are weighed to determine the dry mass m_s. The granite specimen's density and porosity can be articulated as:

$$n = \frac{100(m_{sat} - m_s)}{m_{sat} - m_w}\%$$

(1)

$$\rho_d = \frac{m_s}{m_{sat} - m_w}\rho_w$$

(2)

where n signifies porosity, ρ_d represents dry density, m_{sat} is the post-saturation mass, m_w is the saturated specimen's mass in water, m_s indicates dry mass, and ρ_w denotes the density of water.

Utilizing ultrasonic pulse transmission technology, the P-wave velocity of the samples before heating and after cooling was measured using a Panasonic FZ-G1 acoustic detector, with the sample positioned centrally between two sensors. Vaseline was applied to the interface between the sample and the transducers to ensure efficient energy transfer between them. Moreover, a constant pressure was applied to the

sensors to achieve close contact with the sample. To ensure the reliability of the measurements, three sets of longitudinal wave velocity were recorded under each treatment condition, and their average value was calculated to represent the final P-wave velocity.

In this experiment, the Transient Plane Source (TCS) method is selected to measure the thermal conductivity of granite, which offers advantages such as non-destructiveness, high accuracy, and precision, and does not require any special preparation of the samples prior to testing. The working principle involves heating a semi-infinite body through a moving point heat source and causing a change in the temperature field of the semi-infinite body as it moves relative to it. An infrared temperature sensor records the temperature change, which is related to the thermal conductivity of the granite.

2.4 Mechanical property testing

Mechanical tests were conducted on the GCTS Electro-Hydraulic Servo Rock Mechanics Testing System. This mechanical testing system comprises a loading system, a measurement system, and a control system, enabling precise measurements of the mechanical characteristics of samples under conventional triaxial compression.

The compressive strength of the specimens was determined through triaxial compression tests. At the beginning of the test, a confining pressure of 20 MPa was applied at a rate of 1 MPa/min. Then, axial strain control was adopted at a rate of 0.001%/min until the sample failed, thus obtaining the rock parameters of the sample. Axial and lateral strains were measured using Linear Variable Differential Transformer (LVDT). The measuring range for both axial and lateral LVDT was 6 mm, with an accuracy of 0.0001 mm. Before testing, both LVDT were carefully calibrated.

Furthermore, tensile strength tests on rocks were conducted using the Brazilian Splitting method, employing granite disk samples for this investigation. The disk specimens were subjected to a consistent loading rate of 0.005 mm/min until failure. The Brazilian Tensile Strength (BTS) can be defined as:

$$\sigma_t = \frac{2P}{\pi dt}$$

(3)

where σ_t represents the BTS, P is the load at failure, d denotes the diameter of the disk specimen, and t signifies the thickness of the disk specimen.

2.5 Permeability testing

Because granite is characterized by a dense texture, and the transient pulse permeability testing method is typically used for low-permeability compact rocks, the pulse decay method was employed for permeability measurements. In the test experiment, two gas chambers were connected to the upstream and downstream ends of the specimen, and confining pressures of 2, 4, 5, 10 and 15 MPa were applied sequentially, with the deviatoric stress maintained at 1 MPa. Helium gas was then introduced until the pressures in the upstream and downstream gas chambers equalized and reached equilibrium. While keeping the fluid pressure at the inlet constant, the fluid pressure at the outlet was instantaneously released, creating an initial pressure differential between the two ends. Continuous monitoring of the gas chamber pressures at both ends of the specimen yielded data used to calculate the permeability under the given stress condition:

$$K = -\frac{\mu S L_s}{P_m A_s \left(\frac{1}{V_1} + \frac{1}{V_2}\right)} \tag{4}$$

$$S = \ln(\Delta p_D)/T \tag{5}$$

where K is the permeability; μ is the gas viscosity coefficient, L_s is the specimen height, P_m is the average pressure in the upstream and downstream chambers after completion, A_s is the cross-sectional area of the specimen, V_1 and V_2 are the volumes of the upstream and downstream gas chambers, respectively. S is the slope of the linear regression, Δp_D is the ratio of the final to initial pressure difference, and T is the test duration.

2.6 Microstructural analysis

The observation of microscopic fractures and pores in granite was conducted using CT technology with micrometric precision. The scan had a resolution of 15.6 μm, with the specimen being a cylinder measuring 50 mm in diameter and 100 mm in height. The scanning area spanned approximately 60 mm in height, with a scan interval of 20 μm per slice. Each test yielded approximately 3000 valid two-dimensional cross-sectional slices. Subsequently, the digital images were reconstructed using the image processing software Avizo. Additionally, to ascertain the evolution patterns of pore of different aperture sizes within the granite following high-temperature treatment, NMR was employed to examine the micro-pore distribution within the granite samples.

3 Experimental results

3.1 Physical properties

3.1.1 Density

The changes in the density of rocks under different temperature treatments can indicate the degree of structural loosening and deterioration in mechanical strength. Figure 2 depicts the density variations of granite samples before and after various temperature treatments. Following heating and LN$_2$ cooling treatments, the density of all granite specimens decreased, and the rate of density change exhibited a negative exponential relationship. In this study, the change rate refers to the difference in a sample's property before and after thermal treatment relative to its value before the heat load. Based on the magnitude of the decrease in density, the temperature range of 25–600 °C was divided into three phases. The first phase spanned from 25 to 200 °C; within this phase, the temperature exerted almost no effect on the granite's density, resulting in a minimal change rate. The second phase ranged from 200 to 500 °C, where the granite's density became increasingly influenced by rising temperatures, with a density reduction rate reaching 0.82% at 500 °C. During the third phase, ranging from 500 to 600 °C, the density of the granite declines rapidly, with the reduction rate reaching its peak. At 600 °C, the rate of decrease in density is 1.56%. This indicates that temperature has the most pronounced effect on the density within this phase.

Fig. 2 Density variation of granite samples versus temperature before and after thermal treatment
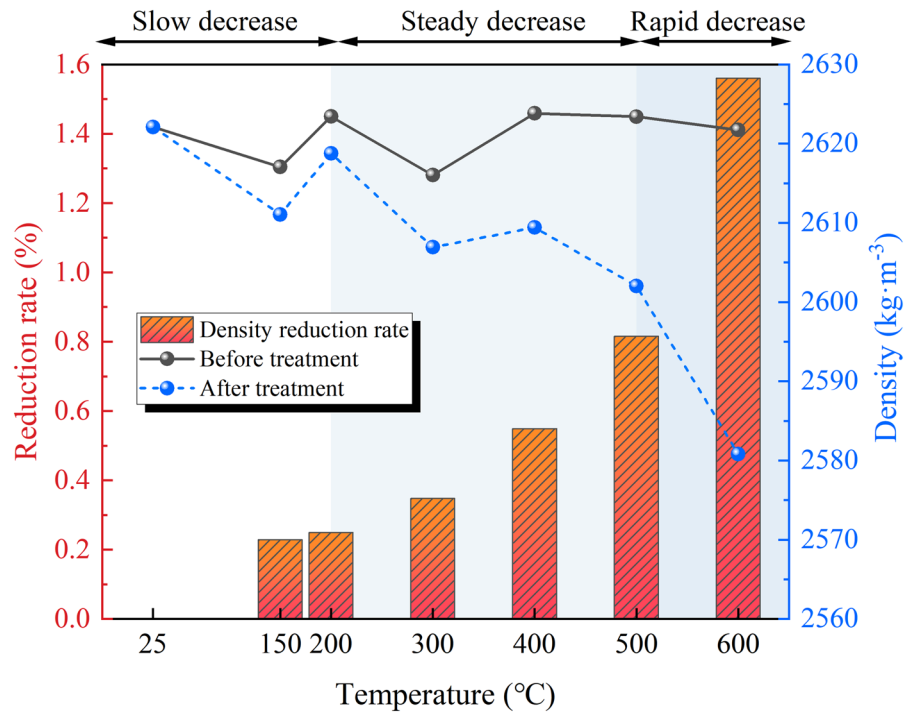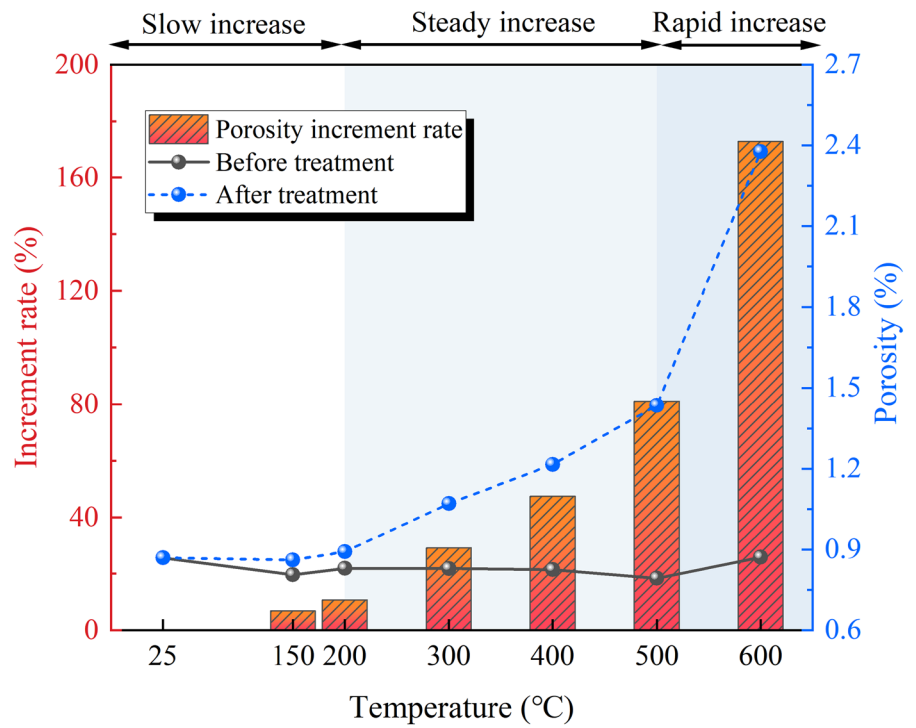

Fig. 3 Porosity variation of granite samples versus temperature before and after thermal treatment

3.1.2 Porosity

Porosity is a fundamental physical attribute of rock, indicating the compactness of its internal structure and significantly influencing the rock's strength and deformation characteristics. Figure 3 depicts the variations in granite specimen porosity before and after distinct temperature treatments. Post-heating and LN_2 cooling procedures, all granite samples displayed a reduction in porosity, with the rate of porosity alteration demonstrating a positive exponential relationship with temperature. Based on the magnitude of the porosity increase, the temperature range of 25–600 °C is segmented into three phases. The first phase encompasses 25–200 °C, within which the temperature has a relatively gentle impact on the increase in granite's porosity, registering a 10.73% augmentation in porosity rate at 200 °C. The second phase, ranging from 200 to 500 °C, manifests an intensified influence on granite porosity alterations due to increasing temperature, culminating in an 81.07% increment in the porosity rate at 500 °C. The third phase, spanning 500–600 °C, showcases the most rapid surge in granite porosity rate, with the impact of temperature on the rate of change being the most pronounced; at 600 °C, the porosity growth rate reached 172.90% compared to untreated specimens.

3.1.3 P-wave velocity

The P-wave velocity test has been extensively utilized to characterize thermal cracking in rocks and to assess internal rock damage. Given that the propagation speed of P-waves in solid media is significantly greater than in air, the evolution of micro-cracks due to thermal damage can be represented through the P-wave velocity. Figure 4 depicts the variation in P-wave velocity of granite samples before and after various thermal treatments. Upon heating and subsequent LN_2 cooling, all granite specimens exhibited a decrease in their P-wave velocity, with the rate of this decline exhibiting a negative exponential relationship. Based on the magnitude of the decrease in P-wave velocity, the temperature range of 25–600 °C is categorized into three phases. The initial phase, spanning 25–200 °C, witnessed a relatively inconspicuous decline in the granite's P-wave velocity, registering a decay of 12.75% at 200 °C. The second phase, from 200 to 500 °C, revealed that as the temperature increased,

Fig. 4 P-wave variation of granite samples versus temperature before and after thermal treatment
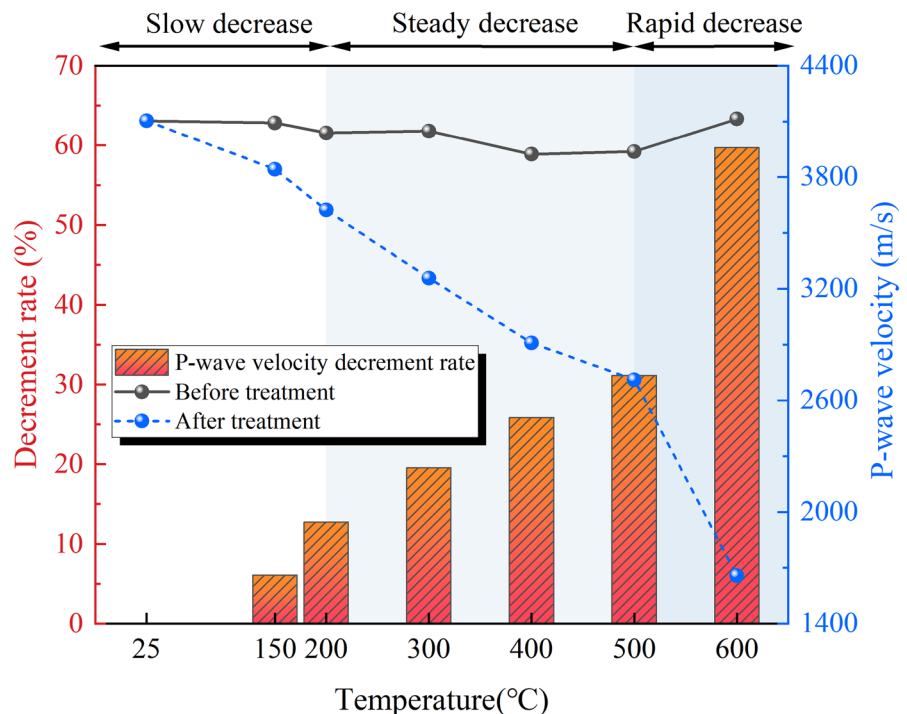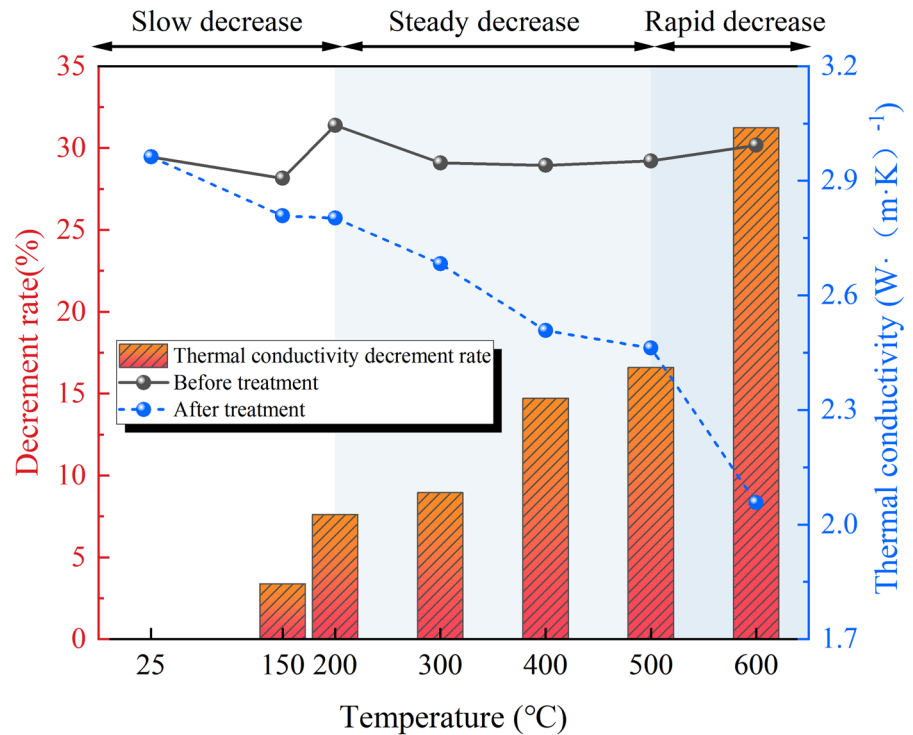
Fig. 5 Thermal conductivity variation of granite samples versus temperature before and after thermal treatment

the impact on the P-wave velocity became more pronounced, culminating in a decay rate of 31.15% at 500 °C. In the third phase, spanning from 500 to 600 °C, the effect of temperature on the P-wave velocity of granite is most conspicuous. At 600 °C, the decrease in the P-wave velocity reaches 59.71%.

3.1.4 Thermal conductivity

In geothermal energy extraction, the thermal conductivity characteristics of reservoir are crucial for the efficiency of geothermal extraction. Figure 5 illustrates the variation in thermal conductivity coefficients of granite samples before and after exposure to different temperatures. After being subjected to heating and LN_2 cooling, the thermal conductivity coefficients of all granite samples decrease, and the rate of change in the thermal conductivity coefficient exhibits a negative exponential relationship. Based on the extent of the decrease in thermal conductivity, the temperature range of 25–600 °C is divided into three phases. During the first phase (25–200 °C), the decay of the granite thermal conductivity coefficient is slow with respect to temperature. In the second phase (200–500 °C), the effect of temperature on the variation of granite's thermal conductivity coefficient increases, and by 500 °C, the rate of change in the thermal conductivity coefficient has decreased by 16.60%. In the third phase (500–600 °C), the rate of change of granite's thermal conductivity coefficient decreases the fastest, with the most significant impact of temperature on the rate of change, and at 600 °C, the thermal conductivity coefficient reduction rate reaches 31.25%.

3.2 Mechanical properties

3.2.1 Stress–strain curves

The complete stress–strain curve of rock samples under triaxial compression tests can be divided into five stages. Under triaxial compression conditions, the axial stress-axial strain curve of rock can be categorized into: (1) crack closure stage, (2) elastic deformation stage, (3) stable crack propagation stage, (4) unstable crack propagation stage, and (5) post-peak deformation stage. The deviatoric stress versus axial, circumferential, and volumetric strain curves for granite samples subjected to different heating and cooling treatments are depicted in Figs. 6, 7 and 8,
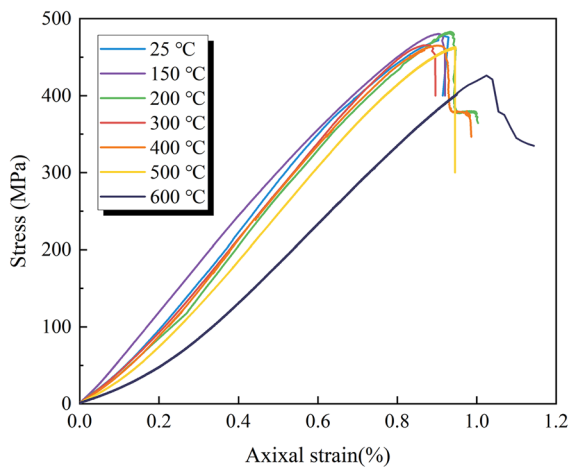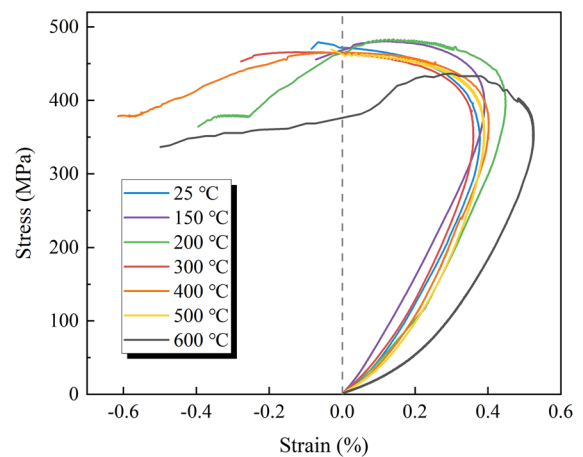
Fig. 6 Stress-axial strain curve

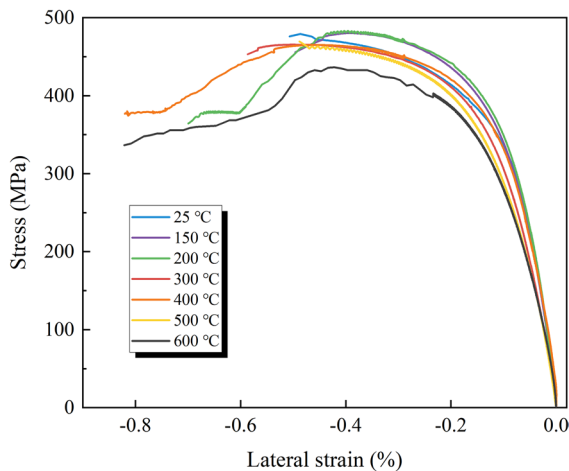

Fig. 8 Stress-volumetric strain curve

Fig. 7 Stress-circumferential strain curve

respectively. The axial stress-axial strain curve exhibits concavity in the initial loading stage. This nonlinear deformation of the rock is associated with the closure of thermally-induced microcracks within the rock during the loading process (Yang et al. 2017). As the temperature increases, the extent of concavity during the initial compaction phase gradually becomes more pronounced. Furthermore, as discerned from Figs. 7 and 8, granite subjected to higher thermal treatment temperatures exhibits more pronounced volumetric compression. These observations suggest that the elevation in thermal treatment temperatures leads to the

formation of an increased number of thermal cracks within the granite. Following the crack closure phase is the elastic deformation phase, where axial stress increases linearly with axial strain. It's generally perceived that during this phase, no new micro-cracks are formed, and elastic modulus of the rock can be determined by the slope of this phase curve. With a further increment in axial load, the stress–strain curve gradient begins to diminish, indicating the onset and stable evolution of new micro-cracks within the specimen. The fourth phase is characterized by unstable crack development, where the growth of microcracks within the rock undergoes a qualitative change, resulting in the formation of pronounced macroscopic cracks, and the deformation behavior is dominated by dilatancy. Subsequently, the specimen reaches its peak strength and transitions into the post-peak deformation phase. Evident from Fig. 6, temperature considerably impacts the specimen's post-peak deformation. Within 200 °C, all granite samples exhibit a sudden stress drop after reaching peak stress, indicating their failure in a brittle manner. Beyond 200 °C, as the treatment temperature escalates, the peak strain incrementally rises, and the post-failure phase shifts from an abrupt drop to a stepped descent. Specimens transition from brittle failure to a more ductile form, with post-peak softening deformation becoming increasingly evident. This suggests a transformation from brittleness to ductility in granite as the temperature elevates.
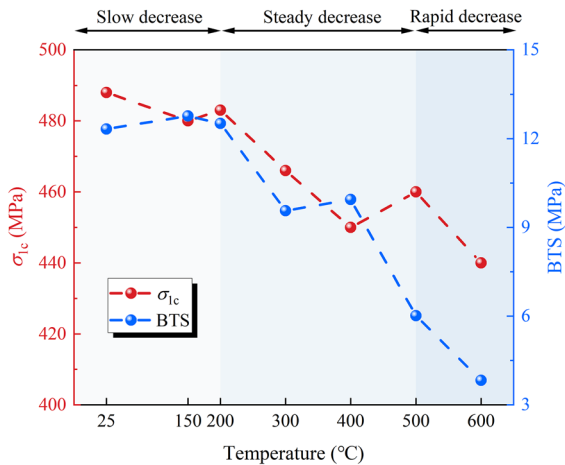
Fig. 9 Variation in σ_{1c} and BTS of granite post LN$_2$ cooling with temperature

Fig. 10 Variation of elastic modulus and Poisson's ratio of granite post LN$_2$ cooling with temperature

3.2.2 Strength characteristic

Figure 9 shows the changes in triaxial compressive strength (σ_{1c}) and BTS after thermal treatment at different temperatures. As the temperature rises from 25 to 200 °C, the decrease in peak strength is not significant, only dropping by 1.02%. With increasing temperature, the peak strength rapidly declines, and at 600 °C, the peak strength reaches its lowest point, representing just 9.84% of the intact sample. Meantime, as the target heating temperature increases, the BTS exhibits a decreasing trend. The BTS decreases very slowly between 25 and 200 °C. Only when the heating temperature exceeds 200 °C does the BTS decrease significantly. At a target heating temperature of 600 °C, the BTS of granite under LN$_2$ cooling decreases by 67.5%.

It can be observed that the deterioration of BTS in granite under the same temperature treatment is more pronounced than the decline in compressive strength, with BTS dropping by 67.5% at 600 °C treatment. This is because granite is a brittle material, with tensile stress being lower than any other types of stress. Moreover, studies conducted by Pai et al. (2021) indicate that transient thermal stresses caused by rapid cooling primarily affect the outer surface of the granite, with the maximum thermal stress being predominantly dominated by vertical thermal stress. This implies that the tensile properties of rocks are more sensitive to microstructural damage than compressive properties.
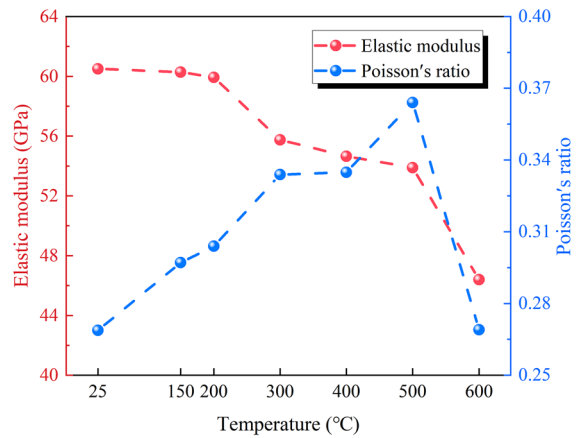
3.2.3 Deformation characteristic

The elastic modulus of rock is a key mechanical parameter in the compressive deformation process, directly affecting the rock's ability to resist deformation and reflecting the micro-characteristics of the rock's mineral composition and crystalline structure. Figure 10 reveals a significant impact of temperature on the elastic modulus, with the modulus decreasing gradually as the temperature increases. At temperatures below 200 °C, there is a slight decrease in the elastic modulus, with a reduction of 0.99% compared to untreated samples. However, as the temperature exceeds 200 °C, thermal treatment leads to further deterioration of the elastic modulus, which reaches its lowest value at 600 °C, registering a decline of 23.32% compared to untreated samples.

The Poisson's ratio is defined as the ratio of lateral to axial strain. Figure 10 illustrates the variation of Poisson's ratio with heating temperature. For granite subjected to heating and LN$_2$ cooling treatments, the Poisson's ratio initially increases with the rise in heating temperature and then swiftly decreases at 600 °C. The initial increase in Poisson's ratio is attributed to the transition of granite from brittle to ductile behavior due to the temperature elevation, causing the rock to soften. This can be described by the equation:

$$K = \frac{E}{3(1 - 2v)} \qquad (6)$$

where K is the bulk modulus, E represents the elastic modulus, and v denotes the Poisson's ratio. Based on the equation, it can be inferred that a larger v implies a smaller K, indicating a softer (ductile) material. However, upon reaching 600 °C, due to a phase transition in quartz, one of the primary mineral constituents within the granite, its crystal structure shifts from tetragonal to hexagonal crystalline structures. This alteration in atomic arrangement (Chaki et al. 2008) results in reduced inter-atomic spacings, subsequently leading to a rapid decline in the Poisson's ratio (Wang 2013).

Failure strain is defined as the axial strain corresponding to the peak strength, offering insights into rock deformation characteristics to a certain extent. Figure 6 delineates the variation in failure strain with respect to thermal treatment temperature. The findings reveal conspicuous changes in failure strain due to distinct heating temperatures. Generally, the failure strain of granite specimens augments with temperature escalation, witnessing a precipitous rise in the range of 500–600 °C for all samples. Furthermore, the slope of the stress–strain curve diminishes with rising temperature. This can be ascribed to the enhanced pores and thermal fractures formation within granite as temperature increases. Consequently, at the same stress level, the samples exposed to higher temperatures require greater axial displacement during the compaction stage to close these pores and microcracks. Therefore, the continuously increasing failure strain is primarily attributed to the larger displacements needed during the crack compaction phase, and it also reflects that the increase in temperature endows granite with greater ductility.

3.3 Permeability variation

Thermal stress induced by high temperatures significantly alters the microstructure within the rock, leading to the formation of new thermal cracks and pores, which in turn results in changes in the permeability characteristics of the rock.

Figure 11 illustrates the permeability of samples at varying temperatures. As the initial temperature elevates, the permeability of rock specimens
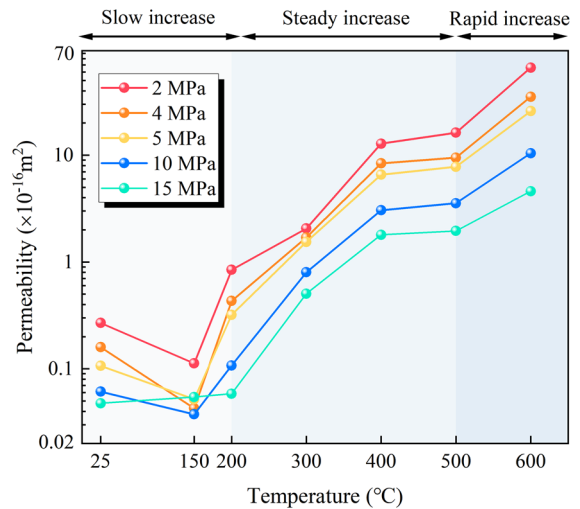

Fig. 11 Three distinct phases of permeability trend following treatment at 25–600 °C

subjected to LN_2 treatment notably increases. During the initial phase ranging from 25 to 200 °C, there's a gradual rise in permeability. Under a confining pressure of 2 MPa at 200 °C, the permeability of the sample increased by 2.14 time compared to the untreated specimen. As the confining pressure increases, the growth rate of permeability slows down at each stage, with the permeability of the 200 °C sample only increasing by 0.18 time compared to the untreated sample under a confining pressure of 20 MPa. The main reasons for these observations are as follows:

(1) Within 200 °C, due to the small temperature gradient, the closure of pores and thermal cracks during heating weakens the expansion of some cracks caused by thermal shock during cooling, so the overall increase in the number and openness of seepage pathways is not significant, leading to slow growth of permeability during this stage.

(2) As the temperature rises, free water and bound water escape, opening flow channels, but confining pressure and thermal expansion close these channels (Ding et al. 2022).

(3) The increase in temperature causes softening of some of the solid framework, affecting the connectivity of flow channels (Feng et al. 2018).

As the temperature continues to rise from 200 to 500 °C, the permeability increases rapidly. At a confining pressure of 2 MPa, the permeability of the sample treated at 500 °C is 1.62×10^{-15} m^2, which is two orders of magnitude greater than untreated specimen. This is due to the fact that thermal stress exceeds the bonding force between mineral particles, resulting in thermal fracturing, and volume and surface area of the total pore-fracture structure increase rapidly with temperature. Consequently, the number and connectivity of flow channels within the sample are enhanced. When the temperature reaches the third stage at 600 °C, the permeability growth rate reaches its maximum. At 2 MPa, the permeability is 6.60×10^{-15} m^2, which is 244 times greater than that at room temperature. This can be attributed to the phase transition of quartz from α to β, causing a significant expansion of the mineral volume, leading to intergranular and intragranular cracks. Numerous interconnected cracks and secondary cracks appear inside the rock. Additionally, thermal shock causes a large number of minerals to detach from the surface, resulting in an increase in internal voids.

When confining pressure is applied to the sample, cracks and pores deform and close, leading to the suppression of fluid flow channels and a subsequent reduction in permeability. Granite flow channels consist of three types: fractures, pore throats, and pores.

Pores, with their arch-like bearing surfaces, undergo little volume change under compressive stress. Pore throats, subjected to tensile stress and with smaller radii, are more prone to closure when compressed. According to the CT scan results in Sect. 4.1, these two components did not exhibit significant development or expansion under thermal stimulation. Compared to pores and pore throats, fractures, which lack support from the skeletal matrix, are more susceptible to deformation and closure (Chen et al. 2017). The connectivity of fluid flow channels is primarily influenced by the extension and closure of fractures, while pore throats and voids have a lesser impact on permeability compared to fractures. As illustrated in Fig. 12, at various temperature stages, as the confining pressure increases, the decline in permeability at higher confining pressures is less than the decline at lower confining pressures.

4 Microstructural analysis

4.1 CT result

Through CT scanning, the pore and fracture within the rock are extracted to reflect the distribution patterns and geometric characteristics of the internal microstructure of granite after heat treatment.

Fig. 12 Contour map of permeability changes under temperature and confining pressure effects post treatment at 25–600 °C
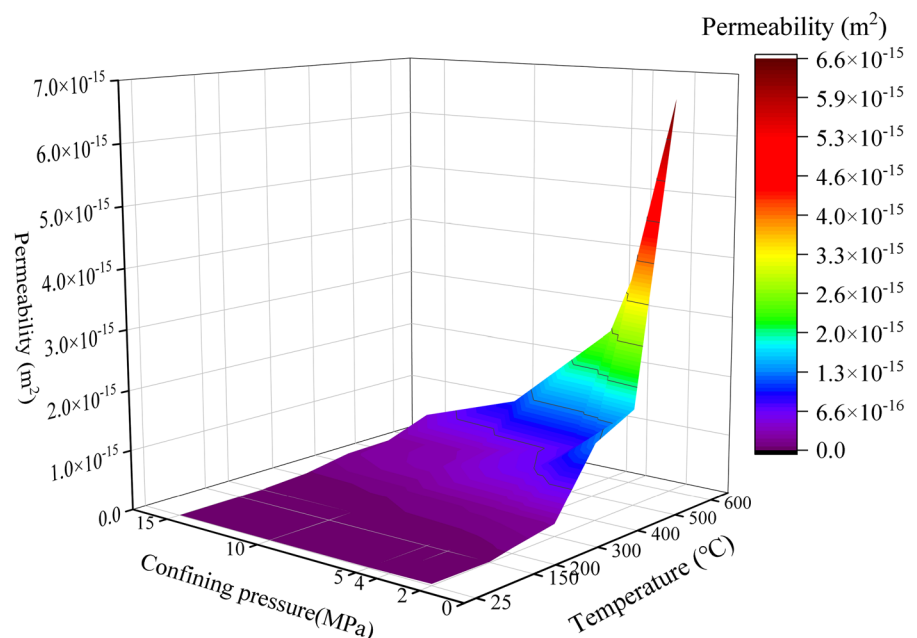
Fig. 13 Volumetric porosity damage ratio variation at different temperatures
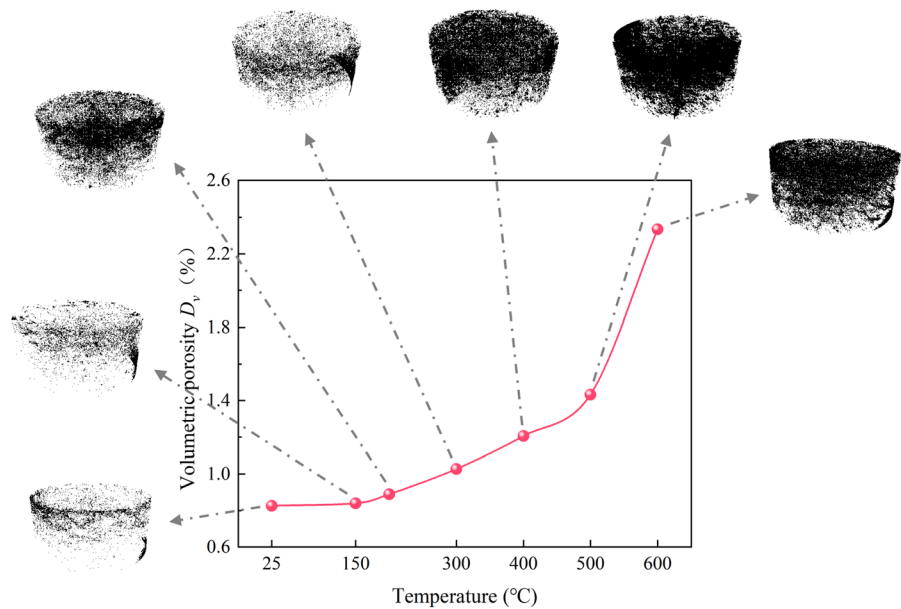

Figure 13 presents a three-dimensional reconstruction of a damaged granite sample, where the black area indicates the damaged region. It can be clearly observed that in the untreated samples, there are few initial pores and fractures. When the temperature is elevated to 200 °C, the damaged area slightly increases, yet the propagation of micro-fractures is not evident. With further temperature increases, the number of thermal fractures steadily rises, and the fractures progressively extend from the external surface to the interior of the sample. At 600 °C, primary fractures accompanied by secondary fractures can be observed, and a significant development of pores is also evident. The volumetric porosity damage ratio (D_v) is introduced to quantitatively assess the thermal shock impact on granite damage. The volumetric porosity damage ratio is the percentage of damaged volume within the analyzed cylindrical sample region relative to the total volume, expressed as:

$$D_v = \frac{V_{\text{Crack + Pore}}}{V_{\text{Total}}} \tag{7}$$

where D_v represents the volumetric porosity damage ratio, V_{Total} is the total volume of the analyzed sample area, and $V_{\text{Pore+Crack}}$ is the volume of cracks and pores within the analyzed sample area. As observed from the Fig. 13, the D_v increases with rising temperatures.

Within 200 °C, the growth of the D_v is not significant. However, beginning at 200 °C, as the temperature increases, the D_v rapidly increases, reaching its maximum growth rate at 600 °C. This trend is consistent with our previous analysis of the variation in physical and mechanical properties under the influence of temperature. Experimental results at the microscopic level confirm that the development of thermally-induced pores and cracks leads to damage in the internal structure of the granite.

To quantitatively evaluate the characteristics of thermal fracture, the fractal method was employed to calculate the fractal dimension of damaged zone. The three-dimensional fractal dimension, which ranges from 2 to 3, effectively reflects the complexity of thermal crack surfaces and quantifies the distribution of thermal cracks within the rock (Li et al. 2023). The rougher the fracture surface and the more complex the pore-fracture structure, the larger the fractal dimension becomes. The fractal dimension is calculated using the box-counting method in three dimensions (Peng et al. 2011):

$$N_{\delta_k} = \sum_{n=1}^{2^{2k}} \left(\frac{\max\left(I(i,j) - \min\left(I(i,j)\right)\right)}{H_k} \right) \tag{8}$$

where $I(i, j)$ is the set of grayscale values for all pixels in the nth box of size δ_k. By employing the least
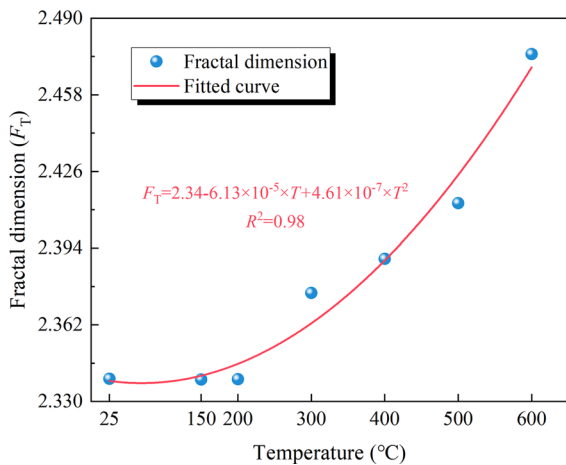
Fig. 14 Three-dimensional fractal dimension variation of granite with temperature

squares method to the scale-independent data points $(-\lg\delta_k, \lg N_{\delta k})$, a linear relationship can be established as:

$$\lg N_{\delta_k} = a \cdot \left(-\lg\delta_k\right) + b \qquad (9)$$

where the slope a represents the three-dimensional fractal dimension. Figure 14 depicts the evolution of fractal dimensions of the fracture network at various temperatures. The results indicate the pronounced fractal characteristics of the thermal fractures, and a clear exponential correlation between the fractal dimension and temperature is evident. At lower temperatures, the fractal dimension increases slowly with rising temperatures, suggesting that temperature changes within 200 °C have a minimal impact on the development and morphology changes of pores and fractures within the granite. As the granite treatment temperature increases, the number and complexity of thermal fractures significantly increase, resulting in a rise in the fractal dimension of the fracture network. Based on the thermal damage mechanism of rock, it is known that the formation, distribution, and expansion of micro-pores and fractures are fundamental factors contributing to the thermal shock damage of granite.

4.2 Mineral composition change

XRD tests can characterize the types and components of rock minerals. As shown in Fig. 15, the granite sample is mainly composed of quartz, oligoclase, biotite, microcline, K-feldspar, montmorillonite, and kaolinite. Among them, microcline, oligoclase, and K-feldspar together constitute more than 90% of the mineral composition. By comparing the diffraction spectra of granite rock samples cooled at different temperatures, it can be observed that there is no significant shift or disappearance of the main mineral diffraction peaks, indicating that the main mineral components have not undergone any fundamental changes. However, temperature has an impact on the mineral content.

Figure 16 illustrates the comparison of mineral content in granite samples subjected to heat treatment at different temperature. When the elevated temperature is below 300 °C, the content of clay minerals (such as kaolinite and montmorillonite) gradually decreases to zero as the temperature increases. This phenomenon is mainly due to the decomposition of clay minerals at temperatures between 200 and 300 °C, leading to a gradual deterioration of the granite's physical and mechanical properties (Liu et al. 2016). In fact, only a few minerals decompose with rising temperatures. In the range of 300–500 °C. The main constituent minerals of granite (such as oligoclase, microcline, and quartz) do not decompose, but this temperature range is sufficient to alter the crystallinity of these minerals (Wu et al. 2019a, b). At high temperatures, the thermal decomposition of biotite intensifies and dehydration melting occurs, with some of the melt crystallizing into irregular K-feldspar (Liu 1998), leading to a decrease in biotite content and an
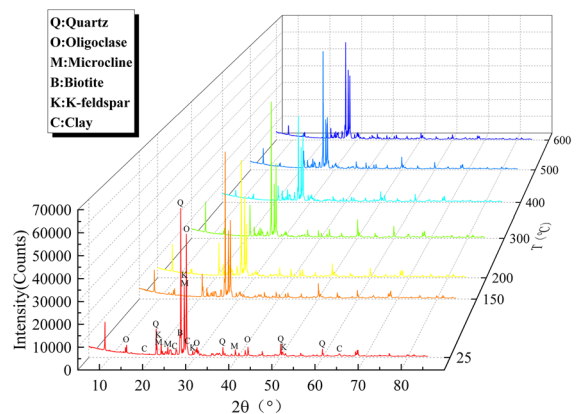

Fig. 15 X-ray diffraction spectra of granite under various temperature treatments
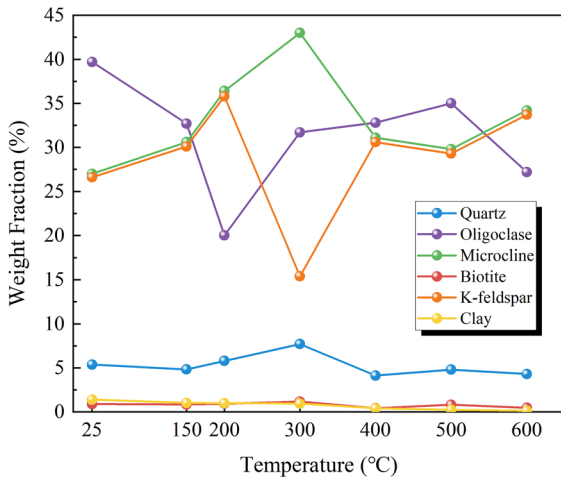
Fig. 16 Variation in mineral composition of granite post high-temperature treatment

increase in K-feldspar content. Li et al. (2020) concluded that in granite subjected to high-temperature treatment, the Young's modulus and hardness of K-feldspar and microcline significantly decreased after exceeding a threshold temperature of 300 °C. The rapid decrease in the overall strength of the granite is primarily due to the reduction in strength and the increased proportion of these minerals within this temperature range. Additionally, the larger the disparity in thermal expansion coefficients between adjacent minerals, the greater the mismatch in deformation, leading to significant localized thermal stresses. This results in the formation of numerous intergranular cracks along the mineral boundaries. This phenomenon is particularly evident at the crystal boundaries of feldspar and quartz, as there is a significant disparity in the thermal expansion coefficients between them. Simultaneously, the release of thermal stresses caused by the high expansion of quartz grains and biotite can also induce intragranular cracking in adjacent feldspar grains (Isaka et al. 2019).

When the temperature is elevated from 500 to 600 °C, the significant alteration of granite's physical and mechanical properties is mainly attributed to the phase transition from α-quartz to β-quartz at 573 °C. In this transition, two Si–O bond angles in the quartz crystal expand to 180°, giving quartz high thermal expansion and anisotropy. This results in a multitude of grain boundary cracks between quartz and adjacent minerals, accelerating the generation of internal

Table 2 Coordinates of peak points of T_2 curve and areas of two peaks after high temperature cycling

T (°C)	P_1			P_2			P_3			Total area
	T_1 (ms)	Signal amplitude (a.u.)	Peak ratio (%)	T_2 (ms)	Signal amplitude (a.u.)	Peak ratio (%)	T_3 (ms)	Signal amplitude (a.u.)	Peak ratio (%)	
25	0.13	1.0996	42.44	6.36	0.9592	33.63	51.11	0.5423	23.92	76.38
150	0.15	0.9203	35.47	11.09	0.9101	44.70	109.69	0.4814	19.81	70.76
200	0.12	0.9312	33.58	6.82	1.3345	46.77	144.81	0.4698	19.64	60.25
300	0.12	0.5530	17.19	13.66	1.5127	82.81	–	–	–	83.61
400	0.14	0.7490	23.97	7.31	1.0427	76.02	–	–	–	83.71
500	0.74	0.9417	45.48	27.36	1.2071	54.51	–	–	–	63.72
600	1.38	0.4532	15.93	16.83	1.5941	84.06	–	–	–	69.73

defects. In summary, high temperatures impact the mineral content of rock, as well as the mechanical properties of minerals, thereby influencing the rock's physical and mechanical parameters.

4.3 Determination of pore structure by NMR test

In NMR testing, the relaxation mechanism of fluids within rock pores primarily consists of three distinct relaxation components: free relaxation, surface relaxation, and diffusion relaxation. The T_2 spectrum in nuclear magnetic resonance testing is a superposition of fluid signals from rock pores of various sizes. Therefore, the T_2 spectrum can reflect the size, quantity, and connectivity of rock pores (Li et al. 2018). Table 2 presents the peak points of the T_2 spectrum curve, along with the corresponding relaxation times and the area proportions of each peak. The unheated sample exhibits a three-peak distribution, and the three peaks are designated as P_1, P_2, and P_3. The untreated sample predominantly consists of micropores. At temperatures below 150 °C, as the temperature rises, the positions and magnitudes of the peaks in the T_2 spectrum remain relatively unchanged, indicating that temperature variations have a minimal impact on the pores within this range. When the temperature reaches 200 °C, the relaxation times of P_2 and P_3 begin to increase, and pore aperture starts to develop and expand. After 200 °C, as the temperature continues to rise, the P_2 peak shifts to the right and merges with P_3, gradually transforming the three-peak curve into a two-peak curve. The T_2 curve steadily increases in height and shifts to the right, indicating that both the quantity and size of granite pores grow with increasing temperature.

T_2 is related to specific surface area (S/V), and the pore radius within the rock can be calculated from the T_2 spectrum using the following formula (Li et al. 2021):

$$\frac{1}{T_2} = \rho_2 \frac{S}{V} = \rho_2 \frac{F_S}{r_c} \tag{10}$$

where ρ_2 is the transverse surface relaxation rate, S and V represent the rock pore surface area and pore volume, respectively. r_c represents the pore radius, and F_S is the shape factor. Drawing on previous research findings, the radius of internal pores in granite is categorized as follows Gu et al. (2023):
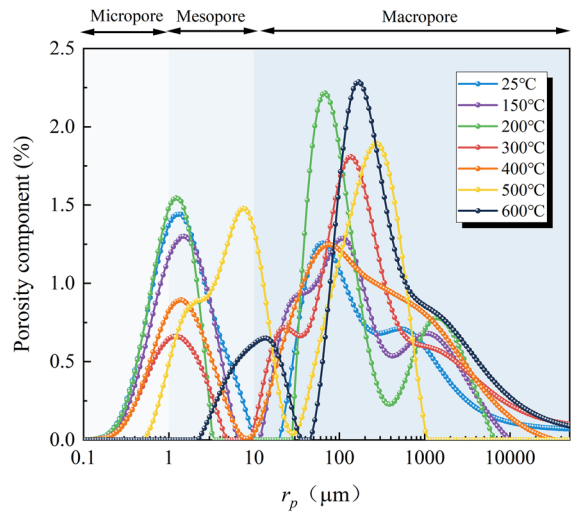

Fig. 17 Variation in pore size distribution of granite at different temperatures

macropore (>10 μm), mesopore (1–10 μm), and micropore (0.1–1.0 μm).

As observed in Fig. 17, within a temperature range of 200 °C, the porosity of granite primarily consists of micropores. The number of micropores slightly increases at 200 °C when compared to the untreated sample. This increase is attributed to the inadequate thermal shock generated by LN$_2$ during the cooling process, which is insufficient to rapidly expand and develop pores (Mo et al. 2022). Beyond 200 °C, the peak value shifts progressively to the right as temperature rises, with the pore size distribution curve gradually moving upward. This shift indicates a transition in pore size from micropores to mesopores and macropores, with a corresponding decrease in micropores and an increase in mesopores and macropores. At 600 °C, micropores essentially disappear, and the number of macropores dramatically increases. This reveals that, under high temperatures, internal micropores in granite gradually grow and interconnect to form mesopores and macropores. Considering the experimental phenomena presented in Sect. 3.3, wherein there's a pronounced decrease in physico-mechanical properties along with a rapid increase in permeability, it can be inferred that another factor contributing to the degradation of the macroscopic physico-mechanical characteristics of granite is the changes in macroporosity. Therefore, the degree

of development of macropores directly influences the damage to granite properties. Furthermore, the amplitude of fluctuations between the dual peaks of the curve increases as the temperature rises, indicating that an increase in temperature enhances the connectivity among the internal pore structures of the rock sample.

5 Discussion

In Sect. 3, we examined the variations in the physico-mechanical properties and permeation characteristics of granite subjected to LN_2 cooling after different temperature treatments. In Sect. 4, we delved into the impact of temperature on its microstructure. In this section, our aim is to analyze the characteristics and mechanisms of thermal damage induced by heating and rapid cooling.

5.1 Characteristic of thermal damage

Different temperature treatments can induce thermal damage to granite, leading to alterations in its physico-mechanical parameters. These properties can be employed to evaluate the extent of thermal damage to the granite. A thermal damage factor is introduced:
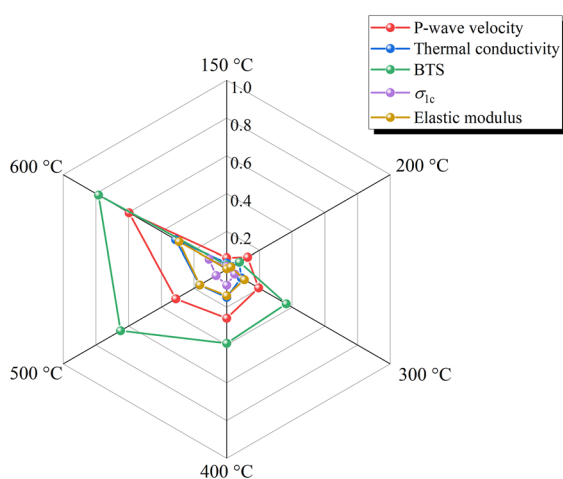
$$D(I) = 1 - \frac{I_T}{I_0} \qquad (11)$$

where $D(I)$ represents the thermal damage factor of granite under varying temperature influences; I_T and I_0 denote the properties of thermally treated granite and untreated granite, respectively. Based on experimental results for physical properties (P-wave velocity, thermal conductivity), mechanical properties (BTS, compressive strength, and elastic modulus), and permeability, the damage state of granite after different temperature treatments is computed.

Figure 18 shows the variation of the thermal damage factor $D(I)$ in granite with the increase in heating temperature. The results indicate that the changes in the thermal damage factors for different properties follow similar trends, with the damage to the granite intensifying as the heating temperature increases. However, the extent of damage based on different physical and mechanical properties is not the same. At different treatment temperatures, the degree of damage to tensile strength is the greatest, followed by the damage to P-wave velocity, thermal conductivity, and elastic modulus, and lastly, the compressive strength. The changes in physical properties mainly manifest in the development of internal pores and the expansion of fractures in the granite, while the reduction in mechanical properties is also due to the softening of the internal skeletal structure of the granite caused by the rise in temperature, leading to different sensitivities to thermal shock damage.

5.2 Mechanisms of thermal damage

The experimental results indicate that an increase in temperature and rapid LN_2 cooling leads to thermal shock damage in granite, which manifests as the development, expansion, and interconnection of pores and fractures within the granite, resulting in the deterioration of its physico-mechanical properties. The subsequent discussion aims to explore the mechanisms of thermal cracking from both heating and cooling perspectives, delving deeper into the impacts of varying heating temperatures and rapid cooling processes on thermal degradation.

As shown in Fig. 19, a series of physico-chemical changes occur in granite as the temperature increases. Below 200 °C, the rise in temperature causes the free water within the granite to vaporize, forming voids
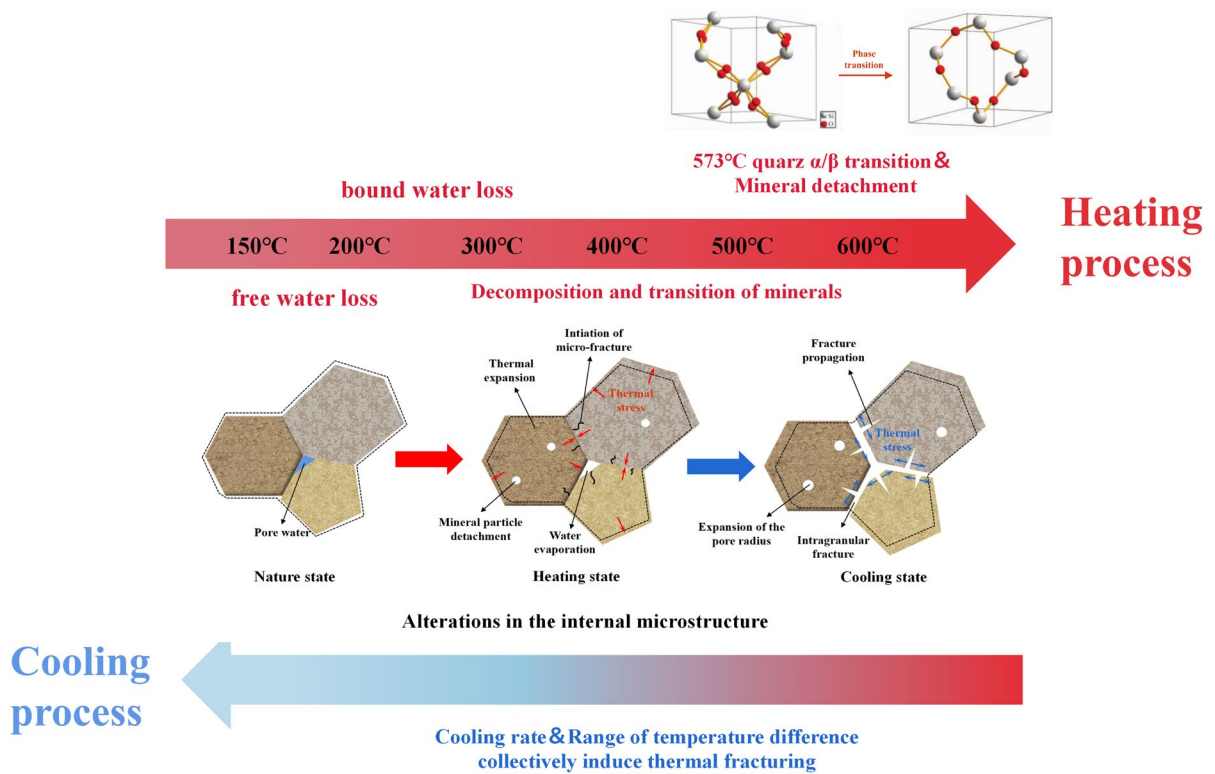

Fig. 18 Variation of thermal damage factor in granite specimens with heating temperature

Fig. 19 Damage mechanisms in granite during heating and cooling processes

(Zuo et al. 2010), and damaging the mineral lattice framework. Additionally, some of the pores are filled due to particle expansion, and during the cooling process, these filled pores may reopen. However, due to the relatively low treatment temperature, the thermal expansion pressure formed during heating is insufficient to generate new fractures, and the thermal stress generated during cooling does not break the bonding strength between minerals, resulting in no noticeable initiation of fracture in this stage, and the development of porosity was manifested in a slight increase in the diameter of micropore, without an increase in their number. However, the absence of an interconnected fracture-pore network implies that the increased pore radius did not enhance the permeation channels, leading to an insignificant increase in permeability.

When the temperature rises from 200 to 500 °C, the free water further evaporates and the crystalline water escapes. The dissociation of H+ and OH− in the mineral lattice structure leads to the destruction of the mineral framework (Zhang et al. 2016). Also,

at high temperatures, rock minerals undergo phase changes and decomposition. Phase transitions usually involve changes in mineral volume, causing localized damage to the internal structure. Decomposition results in reduced mineral content, leading to a decrease in granite strength. Furthermore, granite is a heterogeneous continuum composed of different mineral particles, each with different thermal expansion coefficients. As a result, the mineral particles generate non-coordinated deformation, causing the formation of thermal stress within the granite. When the thermal stress on the mineral particles exceeds the limit, microcracks appear inside the granite. In the 500–600 °C temperature range, the constant loss of mineral particles from the rock sample surface results in a significant increase in voids and a more porous internal structure. At a temperature of 573 °C, quartz grains undergo a phase transition from α to β, with a significant volume increase (Zhang et al. 2017), which further intensifies the loss of mineral particles, consequently resulting in a sharp decline in granite physico-mechanical properties during this phase.

The damage caused during the LN_2 cooling process primarily stems from two factors: cooling rate and temperature differential. Firstly, due to the extremely low temperature of LN_2, it has a very high cooling rate, resulting in intense heat exchange with the high-temperature granite. During cooling, the temperature of granite surface drops rapidly, while the internal cooling rate is slower. This creates a high temperature gradient between the sample's interior and surface, subsequently inducing thermal stress, further deteriorating the thermal damage structure. The tensile stress generated on the exterior exceeds the compressive stress on the interior. As granite has much lower tensile resistance compared to other stress types, and given that granite's tensile strength is significantly weaker than other forms of stress, thermal fractures further develop and expand, exacerbating the formation of macroscopic surface fractures and extending inward, intensifying internal damage. Secondly, thermal damage is related to the temperature difference between LN_2 and the temperature of granite. When the temperature is below 200 °C, the relatively small temperature difference between the granite and LN_2 results in insufficient thermal stress during the cooling process to break the binding strength between minerals, causing minimal damage to the rock structure. However, when the rock temperature is higher, the inter-particle thermal stress caused by LN_2 cooling is significantly greater than the thermal stress generated by cooling rock at lower temperatures. This explains why LN_2 cooling inflicts greater damage on higher temperature granite compared to low-temperature rocks.

5.3 Engineering application

LN_2 fracturing has broad application prospects in enhancing the productivity of HDR geothermal systems. The findings of this study indicate that LN_2 can inflict severe thermal damage to high-temperature granite. This is evident in two main aspects: firstly, it promotes the development and expansion of pore and fracture structures, creating a complex and interconnected network of fractures that enhance the granite's permeability characteristics; secondly, it deteriorates the mechanical properties of granite, thereby reducing the pressure required for fracturing initiation. However, this does not imply that lower temperatures always result in better fracturing effects. Frequent

or sustained cooling may lead to a reduction in the overall temperature of the reservoir, extending the time required for thermal recovery and affecting long-term thermal extraction efficiency. Additionally, LN_2 fracturing might trigger microseismic activities. The high-pressure injection of large volumes of LN_2 into the reservoir increases underground pore pressure, altering the pre-existing stress state of geological strata. If this exceeds the rock's compressive strength, fractures may rapidly propagate, releasing accumulated stress and potentially inducing earthquakes. This risk is particularly acute in geothermal systems with fault structures, where imbalances in strata stress can bring faults to a critical state, making them more prone to slipping—a fundamental mechanism in earthquake occurrence. It is important to note that most earthquakes caused by fracturing are minor. However, the significant temperature differences produced by LN_2 fracturing could lead to stronger earthquakes. Therefore, when employing cooling shock techniques for fracturing, it is imperative to consider both the effectiveness of fracturing and engineering safety comprehensively, in order to optimize the range of temperatures for the cooling shock.

6 Conclusion

In this study, a series of laboratory experiments were conducted to investigate the effects of different heating temperatures under LN_2 cooling on the physical–mechanical properties and seepage characteristics of granite, and to explore the variations in microstructural features. Based on the results, the main conclusions can be summarized as follows:

(1) For granite subjected to LN_2 cooling following exposure to varying temperatures, changes in its physico-mechanical properties occur gradually up to 200 °C. However, when the temperature exceeds 200 °C, there is a rapid decline in the granite's density, P-wave velocity, thermal conductivity, strength, and elastic modulus, accompanied by a substantial increase in porosity and permeability. Moreover, an escalation in confining pressure tends to impede the development of permeability.

(2) The microscale effects of temperature on the internal porosity-fracture structure of granite

were studied through CT scanning and NMR testing. With increasing temperature, the three-dimensional area of microscale defects within the granite expands. micropores gradually grow and connect to form mesopores and macropores, ultimately creating a network of fracture-pore. A quantitative relationship was established between fracture changes and thermal damage in granite. As the temperature rises, the volumetric porosity damage ratio and fractal dimension continuously increase. This demonstrates that higher temperatures promote the growth and development of fractures, intensifying the complexity of the fracture structure. Mineral stability analysis demonstrated that, under elevated temperatures, minerals within the rock experience physico-chemical reactions such as dehydration, phase transitions, and decomposition. These processes modify the mineralogical composition and strength of the minerals.

(3) Thermal cracking mechanisms from the perspectives of both heating and cooling were examined. The rise in temperature leads to the release of free and bound water within the rock, mineral decomposition and phase transitions, and differential thermal expansion among minerals, contributing to thermal damage. During cooling, due to the rapid cooling rate, a temperature gradient forms within the rock, and thermal stress exceeds the mineral bonding strength, causing crack propagation and extension.

Declarations

Ethics approval and consent to participate Not applicable.

Consent for publication All authors have confirmed the publication of this article.

Competing interests The authors declare that they have no known competing financial interests or personal relationships that could have appeared to influence the work reported in this paper.

References

Anderson A, Rezaie B (2019) Geothermal technology: trends and potential role in a sustainable future. Appl Energy 248:18–34. https://doi.org/10.1016/j.apenergy.2019.04.102

Asai P, Panja P, Mclennan J, Deo M (2019) Effect of different flow schemes on heat recovery from enhanced geothermal systems (EGS). Energy 175:667–676. https://doi.org/10.1016/j.energy.2019.03.124

Breede K, Dzebisashvili K, Liu X, Falcone G (2013) A systematic review of enhanced (or engineered) geothermal systems: past, present and future. Geothermal Energy 1:1–27. https://doi.org/10.1186/2195-9706-1-4

Cai C, Li G, Huang Z, Shen Z, Tian S, Wei J (2014) Experimental study of the effect of liquid nitrogen cooling on rock pore structure. J Nat Gas Sci Eng 21:507–517. https://doi.org/10.1016/j.jngse.2014.08.026

Chaki S, Takarli M, Agbodjan WP (2008) Influence of thermal damage on physical properties of a granite rock: porosity, permeability and ultrasonic wave evolutions. Constr Build Mater 22(7):1456–1461. https://doi.org/10.1016/j.conbuildmat.2007.04.002

Chen Y, Wang S, Ni J, Azzam R, Fernandez-Steeger TM (2017) An experimental study of the mechanical properties of granite after high temperature exposure based on

mineral characteristics. Eng Geol 220:234–242. https://doi.org/10.1016/j.enggeo.2017.02.010

Ding Q, Wang P, Cheng Z (2022) Permeability evolution of fractured granite after exposure to different high-temperature treatments. J Petrol Sci Eng 208:109632. https://doi.org/10.1016/j.petrol.2021.109632

Feng G, Kang Y, Chen F, Liu Y, Wang X (2018) The influence of temperatures on mixed-mode (I+ II) and mode-II fracture toughness of sandstone. Eng Fract Mech 189:51–63. https://doi.org/10.1016/j.engfracmech.2017.07.007

Gu Q, Huang Z, Zhong W, Li S, Wu Y, Wu Y (2023) Study on the variations of pore structure and physical and mechanical properties of granite after high temperature cycling. Chin J Rock Mech Eng 42:1450–65. https://doi.org/10.13722/j.cnki.jrme.2022.1024

He C, Mishra B, Shi Q, Zhao Y, Lin D, Wang X (2023) Correlations between mineral composition and mechanical properties of granite using digital image processing and discrete element method. Int J Min Sci Technol. https://doi.org/10.1016/j.ijmst.2023.06.003

Hou P, Su S, Gao F, Liang X, Wang S, Gao Y, Cai C (2022) Influence of liquid nitrogen cooling state on mechanical properties and fracture characteristics of coal. Rock Mech Rock Eng 55(7):3817–3836. https://doi.org/10.1007/s00603-022-02851-6

Hu J, Xie H, Sun Q, Li C, Liu G (2021) Changes in the thermodynamic properties of alkaline granite after cyclic quenching following high temperature action. Int J Min Sci Technol 31(5):843–852. https://doi.org/10.1016/j.ijmst.2021.07.010

Isaka BA, Ranjith PG, Rathnaweera TD, Perera M, De Silva V (2019) Quantification of thermally-induced microcracks in granite using X-ray CT imaging and analysis. Geothermics 81:152–167. https://doi.org/10.1016/j.geothermics.2019.04.007

Jin P, Hu Y, Shao J, Zhao G, Zhu X, Li C (2019) Influence of different thermal cycling treatments on the physical, mechanical and transport properties of granite. Geothermics 78:118–128. https://doi.org/10.1016/j.geothermics.2018.12.008

Kumari WGP, Ranjith PG, Perera MSA, Chen BK (2018) Experimental investigation of quenching effect on mechanical, microstructural and flow characteristics of reservoir rocks: Thermal stimulation method for geothermal energy extraction. J Petrol Sci Eng 162:419–433. https://doi.org/10.1016/j.petrol.2017.12.033

Li H, Li H, Wang K, Liu C (2018) Effect of rock composition microstructure and pore characteristics on its rock mechanics properties. Int J Min Sci Technol 28(2):303–308. https://doi.org/10.1016/j.ijmst.2017.12.008

Li N, Zhang S, Ma X, Zou Y, Li S, Zhang Z (2020) Thermal effect on the evolution of hydraulic fracture conductivity: an experimental study of enhanced geothermal system. J Petrol Sci Eng 187:106814. https://doi.org/10.1016/j.petrol.2019.106814

Li Q, Li X, Yin T (2021) Factors affecting pore structure of granite under cyclic heating and cooling: a nuclear magnetic resonance investigation. Geothermics 96:102198. https://doi.org/10.1016/j.geothermics.2021.102198

Li Z, Ren T, Li X, Qiao M, Yang X, Tan L, Nie B (2023) Multi-scale pore fractal characteristics of differently

ranked coal and its impact on gas adsorption. Int J Min Sci Technol 33(4):389–401. https://doi.org/10.1016/j.ijmst.2022.12.006

Li Z, Xu H, Zhang C (2016) Liquid nitrogen gasification fracturing technology for shale gas development. J Petrol Sci Eng 138:253–256. https://doi.org/10.1016/j.petrol.2015.10.033

Liu F (1998) Textural characteristics and dynamic significance of metamorphic reaction involving melt in khondalite series on the border of Shanxi and Inner Mongolia. Acta Petrol Sin 14(2):129–139

Liu X, Yuan S, Sieffert Y, Fityus S, Buzzi O (2016) Changes in mineralogy, microstructure, compressive strength and intrinsic permeability of two sedimentary rocks subjected to high-temperature heating. Rock Mech Rock Eng 49:2985–2998. https://doi.org/10.1007/s00603-016-0950-z

Mcdaniel BW, Grundmann SR, Kendrick WD, Wilson DR, Jordan SW (1997) Field applications of cryogenic nitrogen as a hydraulic fracturing fluid. In: SPE Annual technical conference and exhibition. Society of Petroleum Engineers

Mo C, Zhao J, Zhang D (2022) Real-time measurement of mechanical behavior of granite during heating–cooling cycle: a mineralogical perspective. Rock Mech Rock Eng 55(7):4403–4422. https://doi.org/10.1007/s00603-022-02867-y

Pai N, Feng J, Haijian S, Zequan H, Meng X, Yazhen Z, Cheng Z, Dong W (2021) An investigation on the deterioration of physical and mechanical properties of granite after cyclic thermal shock. Geothermics 97:102252. https://doi.org/10.1016/j.geothermics.2021.102252

Pan S, Gao M, Shah KJ, Zheng J, Pei S, Chiang P (2019) Establishment of enhanced geothermal energy utilization plans: barriers and strategies. Renew Energ 132:19–32. https://doi.org/10.1016/j.renene.2018.07.126

Peng R, Yang Y, Ju Y, Mao L, Yang Y (2011) Computation of fractal dimension of rock pores based on gray CT images. Chin Sci Bull 56:3346–3357

Sha S, Rong G, Chen Z, Li B, Zhang Z (2020) Experimental evaluation of physical and mechanical properties of geothermal reservoir rock after different cooling treatments. Rock Mech Rock Eng 53:4967–4991. https://doi.org/10.1007/s00603-020-02200-5

Sun H, Sun Q, Deng W, Zhang W, Lü C (2017) Temperature effect on microstructure and P-wave propagation in Linyi sandstone. Appl Therm Eng 115:913–922. https://doi.org/10.1016/j.applthermaleng.2017.01.026

Tang ZC, Sun M, Peng J (2019) Influence of high temperature duration on physical, thermal and mechanical properties of a fine-grained marble. Appl Therm Eng 156:34–50. https://doi.org/10.1016/j.applthermaleng.2019.04.039

Ulusay R, Hudson JA (2007) International Society for Rock Mechanics (ISRM), the complete ISRM suggested methods for rock characterization, testing and monitoring, 1974–2006. Ankara, Oxford, Pergamon

Wang L, Yao B, Cha M, Alqahtani NB, Patterson TW, Kneafsey TJ, Miskimins JL, Yin X, Wu Y (2016) Waterless fracturing technologies for unconventional reservoirs-opportunities for liquid nitrogen. J Nat Gas Sci Eng 35:160–174. https://doi.org/10.1016/j.jngse.2016.08.052

Wang W (2013) The nature and properties of amorphous matter. Prog Phys 33(5):177–351

Wu X, Huang Z, Cheng Z, Zhang S, Song H, Zhao X (2019a) Effects of cyclic heating and LN2-cooling on the physical and mechanical properties of granite. Appl Therm Eng 156:99–110. https://doi.org/10.1016/j.applthermaleng.2019.04.046

Wu X, Huang Z, Li G, Li R, Yan P, Deng X, Mu K, Dai X (2018) Experiment on coal breaking with cryogenic nitrogen jet. J Petrol Sci Eng 169:405–415. https://doi.org/10.1016/j.petrol.2018.05.061

Wu X, Huang Z, Song H, Zhang S, Cheng Z, Li R, Wen H, Huang P, Dai X (2019b) Variations of physical and mechanical properties of heated granite after rapid cooling with liquid nitrogen. Rock Mech Rock Eng 52:2123–2139. https://doi.org/10.1007/s00603-018-1727-3

Wu Y, Tao J, Wang J, Zhang Y, Peng S (2021) Experimental investigation of shale breakdown pressure under liquid nitrogen pre-conditioning before nitrogen fracturing. Int J Min Sci Technol 31(4):611–620. https://doi.org/10.1016/j.ijmst.2021.05.006

Xie Y, Wu X, Hou Z, Li Z, Luo J, Lüddeke CT, Huang L, Wu L, Liao J (2023) Gleaning insights from German energy transition and large-scale underground energy storage for China's carbon neutrality. Int J Min Sci Technol. https://doi.org/10.1016/j.ijmst.2023.04.001

Yang S, Ranjith PG, Jing H, Tian W, Ju Y (2017) An experimental investigation on thermal damage and failure mechanical behavior of granite after exposure to different high temperature treatments. Geothermics 65:180–197. https://doi.org/10.1016/j.geothermics.2016.09.008

Zhang W, Sun Q, Hao S, Geng J, Lv C (2016) Experimental study on the variation of physical and mechanical properties of rock after high temperature treatment. Appl Therm Eng 98:1297–1304. https://doi.org/10.1016/j.applthermaleng.2016.01.010

Zhang Y, Sun Q, He H, Cao L, Zhang W, Wang B (2017) Pore characteristics and mechanical properties of sandstone under the influence of temperature. Appl Therm Eng 113:537–543. https://doi.org/10.1016/j.applthermaleng.2016.11.061

Zhu ZN, Tian H, Dong NN, Dou B, Chen J, Zhang Y, Wang BH (2018) Experimental study of physico-mechanical properties of heat-treated granite by water cooling. Rock Soil Mech 39(Suppl 2):169. https://doi.org/10.16285/j.rsm.2018.0967

Zuo J, Xie H, Zhou H, Peng S (2010) SEM in situ investigation on thermal cracking behaviour of Pingdingshan sandstone at elevated temperatures. Geophys J Int 181(2):593–603. https://doi.org/10.1111/j.1365-246X.2010.04532.x

Publisher's Note Springer Nature remains neutral with regard to jurisdictional claims in published maps and institutional affiliations.